15th World Congress on Computational Mechanics (WCCM-XV)
8th Asian Pacific Congress on Computational Mechanics (APCOM-VIII)
Virtual Congress: 31 July – 5 August 2022
S. Koshizuka (Ed.)

MULTISCALE MODELLING OF NORMAL FAULT RUPTURE-SOIL-FOUNDATION INTERACTION

LIFAN CHEN[1], NING GUO[2] AND ZHONGXUAN YANG[3]

[1] College of Civil Engineering and Architecture, Zhejiang University.
866 Yuhangtang Road, Hangzhou, Zhejiang, 310058, China.
Email: lifanchen@zju.edu.cn

[2] College of Civil Engineering and Architecture, Zhejiang University.
866 Yuhangtang Road, Hangzhou, Zhejiang, 310058, China.
URL: https://person.zju.edu.cn/nguo. Email: nguo@zju.edu.cn

[3] College of Civil Engineering and Architecture, Zhejiang University.
866 Yuhangtang Road, Hangzhou, Zhejiang, 310058, China.
URL: https://person.zju.edu.cn/zxyang. Email: zxyang@zju.edu.cn

Key words: Multiscale modelling, Finite element method, Discrete element method, Normal fault rupture-soil-foundation interaction

Abstract. *A multiscale approach that couples the finite element method (FEM) and the discrete element method (DEM) is employed to model and analyses the earthquake fault rupture-soil-foundation interaction (FR-SFI) problem. In the approach, the soil constitutive responses are obtained from DEM solutions of representative volume elements (RVEs) embedded at the FEM integration points so as to effectively bypass the phenomenological hypotheses in conventional FEM simulations. The fault rupture surfaces and shear localization patterns under normal faults with or without foundation atop have been well captured by the multiscale approach and verified with available centrifuge experimental and numerical results. By examining the responses and microstructural evolutions of local RVE packings, it is found that the RVEs located in- or outside the shear bands (SBs) behave distinctly, and may change their stress states from initial at-rest to active in the normal fault case. The micromechanics study also sheds lights on the possible detriment of heavy foundations for the superstructure despite the rupture surface diversion.*

1 INTRODUCTION

Within earthquake-related hazards, the fault rupture induced permanent ground deformation is among the most devastating threats to human activities and facilities such as buildings, transportation networks, and buried pipelines [1-3]. Avoidance or mitigation of the adverse effects of earthquake fault ruptures is of great importance yet remains challenging due to the complexity of the problem involving fault rupture propagation through soil layers and their possible interactions with sub/super-structures [4, 5].

Comprehensive physical tests were performed by Bransby et al. [6] using centrifuge under an

acceleration of 115 g to investigate the FR-SFI in dry sand considering both normal and reverse dip-slip faults. The high-quality test data have since been extensively used as benchmarks to validate various numerical schemes through back analysis, including FEM [7], FDM [8], SPH [9] and DEM [10-12]. The continuum-based methods commonly need phenomenological hypotheses on the constitutive relations, whereas DEM is difficult to use in boundary value problem (BVP) due to computational efficiency. In this regard, a novel multiscale approach proposed by Guo and Zhao [13] is employed for the present study of FR-SFI, where FEM is used to solve the BVP with each integration point of the mesh embedded a representative volume element (RVE). The material constitutive responses are then derived from DEM solutions of these RVE packings and fed back to FEM, thus bypassing the phenomenological assumptions in traditional continuum-based methods. And a link between the micro- and the macroscales is therefore naturally established by the multiscale approach. Details of the formulation and solution can be found in Guo and Zhao [13].

2 FORMULATIONS IN MULTISCALE METHOD

2.1 FEM

The governing equation for the BVP to be solved by FEM is the balance of momentum equation, which for a quasi-static problem writes

$$\sigma_{ij,j} + b_i = 0 \tag{1}$$

where σ_{ij} is the stress tensor and b_i is the body force, denoting gravity herein. After standard FEM discretization, Eq. (1) can be rewritten in the discrete matrix form

$$\mathbf{Ku} = \mathbf{R} \tag{2}$$

where $\mathbf{K}$ is the stiffness matrix; $\mathbf{u}$ is the unknown nodal displacement vector, and $\mathbf{R}$ is the residual force vector. The internal force is given by

$$\mathbf{f}^{\text{int}} = \int_{\Omega} \mathbf{B}^T \boldsymbol{\sigma} d\Omega \tag{3}$$

where $\mathbf{B}$ is the displacement–deformation matrix and Ω denotes the problem domain. By assembling the material tangent modulus $\mathbf{D}$, $\mathbf{K}$ in Eq. (2) can be reached by

$$\mathbf{K} = \int_{\Omega} \mathbf{B}^T \mathbf{D} \mathbf{B} d\Omega \tag{4}$$

2.2 DEM

The open-source code SudoDEM [14] is employed as the DEM solver. In each RVE, the homogenized Cauchy stress tensor is reached by

$$\sigma_{ij} = \frac{1}{V} \sum_{N^c} f_i^c d_j^c \tag{5}$$

where V is the volume of the RVE; N^c is the number of contacts; f_i^c and d_j^c are the branch vector and the contact force, respectively. The tangent modulus of an RVE packing can be obtained by resorting to the uniform strain assumption [15]

$$D_{ijkl} = \frac{1}{V}\sum_{N^c}\left(k_n n_i^c d_j^c n_k^c d_l^c + k_t t_i^c d_j^c t_k^c d_l^c\right) \tag{6}$$

where n_i^c and t_i^c are the unit vectors along the normal and the tangent directions at a contact, respectively.

Bridging the microstructures and the macroscopic behaviors of materials is an appealing feature of multiscale approach. In this study, the former is characterized by two fabric tensors quantifying the distribution of contact normal and particle orientation, denoted as ϕ_{ij}^c and ϕ_{ij}^p respectively, following Zhao and Guo [16] and Guo et al. [17]. The fabric tensor ϕ_{ij}^* can be reached by

$$\phi_{ij}^* = \int_\Theta E(\Theta) n_i^* n_j^* = \frac{1}{N^*}\sum_{N^*} n_i^* n_j^* \tag{7}$$

where the superscript, '*', can be either 'c' for the contact normal-based fabric or 'p' for the particle orientation-based one. N^p is the number of particles in the RVE packing; n_i^p is the unit vector along the longest axis of a particle; Θ denotes the vector direction in the global coordinate system; $E(\Theta)$ is the probability distribution function. In practice it is convenient to use the deviatoric fabric tensor for discussion, i.e., $F_{ij}^* = 4\left(\phi_{ij}^* - \delta_{ij}/2\right)$ for a 2D case (δ_{ij} = Kronecker delta). A scaler can be used to measure the anisotropic intensity: $F_* = \sqrt{F_{ij}^* F_{ij}^*/2}$.

3 MODEL SETUP

3.1 Preparation of RVEs

A DEM assembly containing 400 particles with radius between 4 mm and 6 mm is used for the RVE. The aspect ratio and density of the particles are 0.75 and 2650 kg/m^3, respectively. 2D case is considered in this study, so all the particles are assumed to have an out-of-plane thickness of 20 cm. A linear contact model similar to Guo et al. [17] is employed using the contact stiffness $k_n = k_t = 6 \times 10^6$ N/m and the inter-particle frictional coefficient $\mu = 0.55$.

The macroscopic mechanical properties (in terms of the friction and dilation angles) of the RVE are checked before applying it to the FR-SFI study. The RVE is first isotropically consolidated to a mean stress of 200 kPa, which is close to the average vertical stress in the whole domain. The resulted RVE packing is illustrated in Fig. 1(a), with superimposed force-chains (the chain widths are proportional to the magnitudes of the normal contact forces), which is indicative of an initial isotropic microstructure. The drained biaxial compression test is then conducted on the RVE with the stress–strain and the dilation curves shown in Fig. 1(b). The peak friction angle ϕ_{max} and the peak dilation angle ψ_{max} can be estimated according to Bolton [18]

$$\sin\phi_{max} = \frac{(\sigma_1/\sigma_3)_{max} - 1}{(\sigma_1/\sigma_3)_{max} + 1} \tag{8}$$

$$\sin\psi_{max} = \frac{(d\varepsilon_1/d\varepsilon_3)_{max} + 1}{1 - (d\varepsilon_1/d\varepsilon_3)_{max}} \tag{9}$$

where σ_1 ($d\varepsilon_1$) and σ_3 ($d\varepsilon_3$) are the major and the minor principal stress (strain increment),

respectively. From Fig. 1(b), the two angles are found to be $\phi_{max} = 30.8°$ and $\psi_{max} = 6.6°$ for the RVE. The values agree reasonably well with those reported in Bransby et al. [6] for Fontainebleau sand with a relative density of 60% ($\phi_{max} = 35°$ and $\psi_{max} = 6°$ therein).

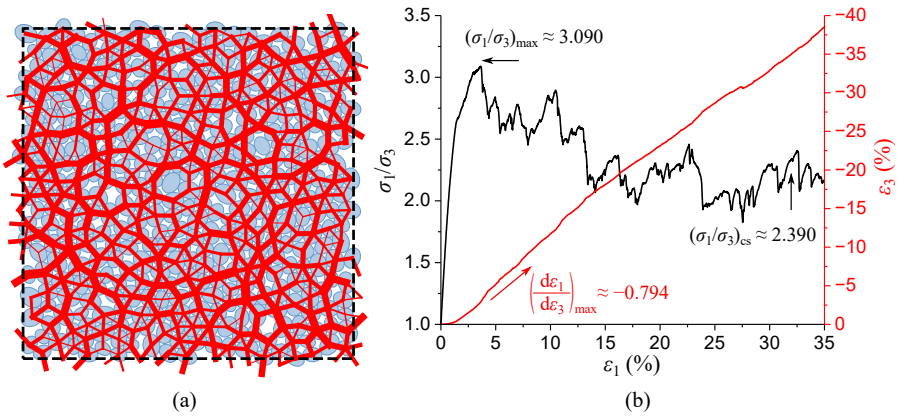

Fig. 1. (a) RVE packing after isotropic consolidation; and (b) drained biaxial compression test results.

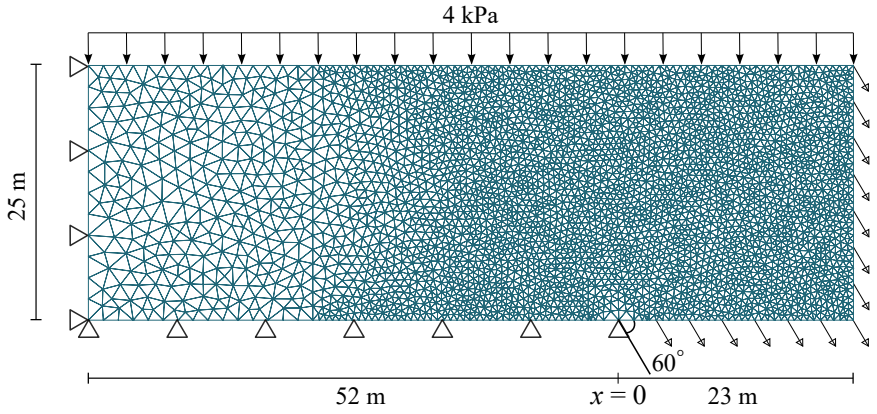

Fig. 2. Meshes and boundary conditions

3.2 FR-SFI model

With the application of Earth's gravity ($1g$), the dimensions of the multiscale simulation model are 75 m in width and 25 m in depth (H) for the normal fault case, following the prototype sizes of the model in the centrifuge experiment [6]. For the boundary condition, the left and the bottom surfaces within 52 m from the left (foot wall boundary) are fixed in space, and the right and the bottom sides over 52 m from the left (hanging wall boundary) are moving with prescribed displacements, downward for the normal fault, as shown in Fig. 2. The dip angle of the bedrock fault displacement is 60°, consistent with the centrifuge experiments [6]. For the sake of numerical stability, a small surcharge load of 4 kPa (~1% of the maximum vertical stress in the normal fault) is applied on the top surface. Shown in Fig. 2, the problem domain is discretized with 7563 linear triangle elements, one integration point for each element.

The soil unit weight is set as $\gamma = 15.68\ \mathrm{kN/m^3}$, the same as Fontainebleau sand with 60%

relative density in Bransby et al. [6]. The coefficient of earth pressure at rest k_0 is found to be around 0.4 after gravity deposition. And the void ratio e throughout the domain is in the range 0.160–0.179. For simplicity, the foundation is treated as a thin rectangular beam and modeled as elastic with the two Lamé parameters $\lambda = 20$ GPa and $G = 12$ GPa and is also assumed to stick to the ground. The additional bearing pressure Q is modeled as the self-weight of the foundation, similar to that in the centrifuge tests.

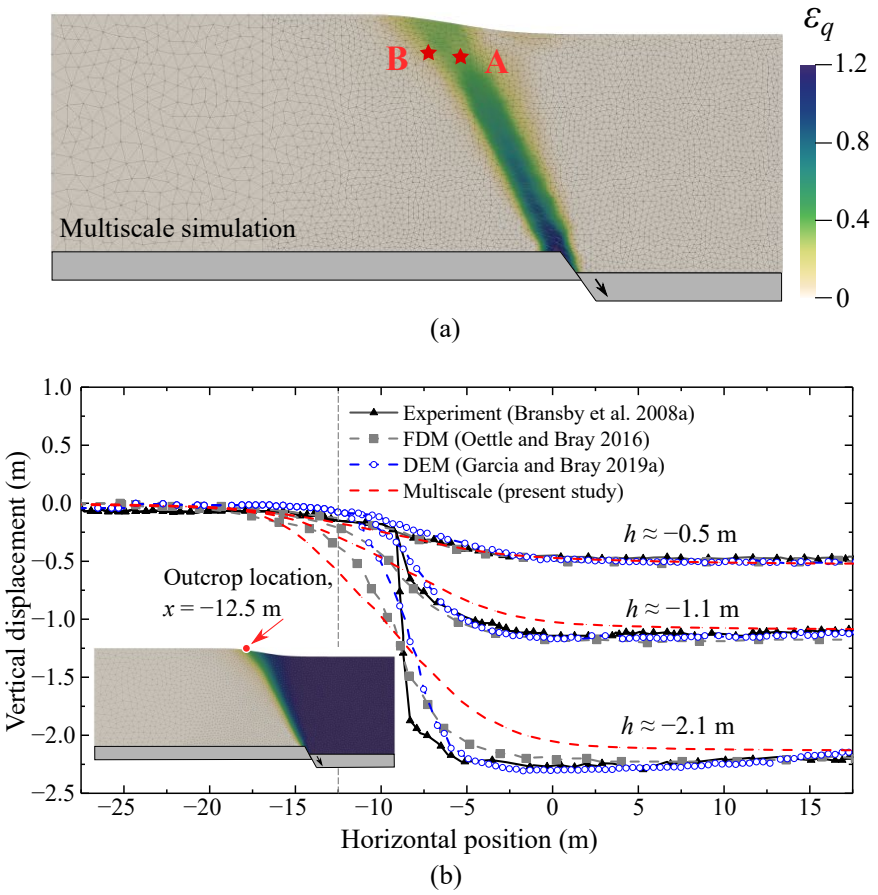

Fig. 3. (a) deformation pattern from multiscale simulation at $h/H = -0.085$; (b) surface displacements among centrifuge experiment by Bransby et al. [6], FDM simulation by Oettle and Bray [8], DEM simulation by Garcia and Bray [11] and multiscale simulation. The inset of (b) shows the vertical displacement contour at $h/H = -0.085$.

4 RESULTS AND DISCUSSION

4.1 Free-field fault rupture

Fig. 3 reports the present multiscale simulation results as well as other numerical results at different fault throw h normalized by the domain depth H, where h is defined as the vertical component of the fault displacement. From Fig. 3(a), the fault rupture has developed through the soil layer and a distinct SB is visible in both experimental and numerical tests at $h/H = -0.085$. However, there is an apparent scarp around the outcrop in the experiment [6], whereas a relatively flat slope is observed in the multiscale simulation (see also Fig. 3(b)). This

difference may result from the additional surcharge applied on the ground in the multiscale simulation and that the present multiscale model fails to capture the physical SB width without introducing any intrinsic material length to regularize its solution [19]. The two RVE packings located at the points A and B marked in Fig. 3(a) are chosen for multiscale analyses to be introduced in the later subsection.

Fig. 3(b) refers to the vertical displacements of the ground surface at three different fault throws from the multiscale simulation and other studies in the literature, including the centrifuge experiment by Bransby et al. [6], the FDM simulation by Oettle and Bray [8], and the DEM simulation by Garcia and Bray [11]. Compared with other results, multiscale simulation predicts the mildest transition from the foot wall to the hanging wall with a slope of minimum inclination and broadest extent. The difference could be attributable to the more contractive RVE behaviors than the other simulations and the experiment. The outcrop location on the ground can be determined as the point where the ground surface starts to deflect and is estimated roughly at $x = -12.5$ m in this normal fault case, which has an offset toward the foot wall side by 2.7 m in contrast to the location from the centrifuge experiment [6] (note the outcrop locates at $x = -9.8$ m therein). The different constitutive responses of natural Fontainebleau sand and numerical models, as well as boundary friction in the experiments [20] may be responsible for the discrepancy.

4.2 FR-SFI results

In this subsection, two centrifuge experimental tests on FR-SFI problems by Bransby et al. [6] is simulated using the multiscale approach. The tested normal fault simulations include a heavy foundation case (foundation width $B = 10$ m with a bearing pressure of $Q = 91$ kPa and a distance between the left edge of the foundation and the outcrop location in free-field $s = 3$ m) and a light foundation case ($B = 10$ m, $Q = 37$ kPa, $s = 3$ m), following Bransby et al. [6]. Since the outcrop location in free-field is estimated at $x = -12.5$ m, the centers of foundations locate at $x = -10.5$ m in the two cases.

Fig. 4 depicts the results of normal fault rupture propagation through soil at $h = -1.99$ m under the heavy and the light foundations. During the process, a major localization band is observed and marked as *S*1, which emanates from the bottom bedrock and the left edge of the foundation on the ground almost simultaneously, and intersects and forms a penetrating failure plane shortly. The diversion of outcrop location from that in free-field is well captured in the multiscale simulation. These observations generally agree with those reported in Bransby et al. [6] and Garcia and Bray [11], only that a secondary and much weaker SB bifurcates from the primary one at the bottom in the centrifuge test (Bransby et al. [6]).

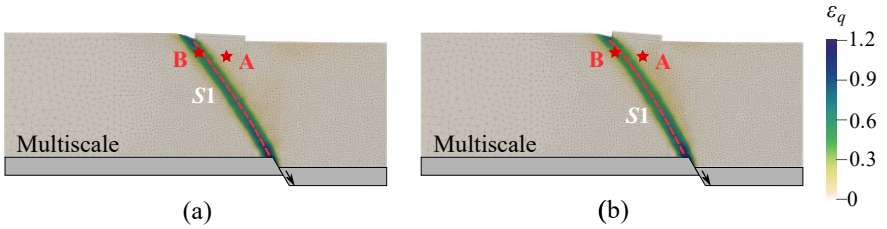

Fig. 4. The normal FR-SFI results at $h = -1.99$ m: (a) heavy; (b) light foundations.

4.3 Multiscale analyses

One appealing feature of multiscale approach lies in its ability to easily conduct cross-scale analyses. In the FR-SFI problem, it has been recognized that the foundation bearing condition imposes a profound influence on fault rupture propagation [6, 8, 11]. To thoroughly interpret the foundation bearing effect on rupture diversion and demonstrate the capability of the method in multiscale analysis, the RVEs at point A and B (see Figs. 3(a) and 4) are selected and their micromechanical responses are analyzed, where Point A is in the SB in the free-field case and point B locates in the shear localization zones in the cases with foundations.

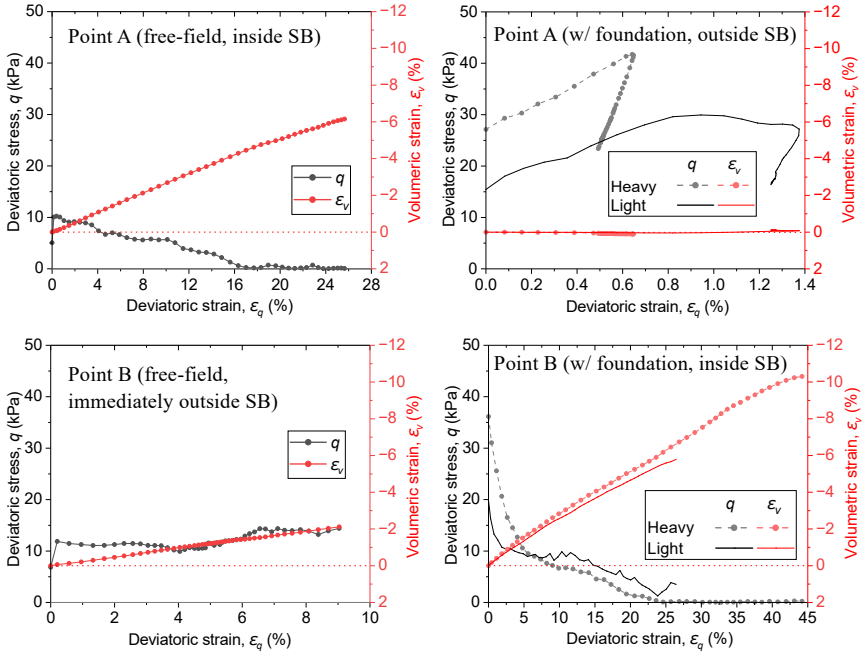

Fig. 5. Mechanical responses of the two selected RVEs embedded at points A and B: (a) free-field; (b) heavy and light foundations.

The deviatoric stress-strain relations and the dilation curves up to $h/H = 0.08$ for these RVEs under different bearing conditions are depicted in Fig. 5. For the RVEs at point A in the free-field and at point B under the light and the heavy foundations which are inside the shear localization zones, these RVEs are all under the active state undergoing sustained volume expansion with final ε_V exceeding −6%. Their deviatoric stress q drops continuously to zero at around $\varepsilon_q = 20\%$. From Fig. 5(b), it is interesting to see that compared with the light foundation case, the RVE at point B under heavy foundation experiences much severer volume expansion ($\varepsilon_V > 10\%$) and more thorough stress relaxation ($q \approx 0$ kPa), indicating heavy foundations could be devastating under normal fault (Garcia and Bray [12]). The shear deformation levels experienced by these RVEs are also large with ε_q exceeding 25%. With overburden foundations, the RVEs at point A gain much larger shear strength. The peak values of q reach 30 kPa and 42 kPa for the light and the heavy foundations, respectively. The volumetric strains of the RVEs are also relatively small. After the peak state, an unloading

process has been observed for the RVEs at point A (Fig. 5(b)). This unloading phenomenon for material points outside the shear localization zones explains the deviation of fault ruptures with the existence of foundations. As for the RVE at point B in the free-field (outside SB), its responses resemble a typical biaxial shear.

Fig. 6 presents the evolution of the two fabric anisotropy measures, F_p and F_c, at the two points for different bearing conditions. The initial values of both measures are small ($F_p \approx 0.03$ and $F_c \approx 0.05$) indicating a slightly anisotropic microstructure of the RVE packings under gravity. Upon fault rupturing, the contact normal-based fabric F_c increases swiftly whereas the particle orientation-based fabric F_p evolves much gently. For the free-field condition, the RVE at point A inside SB has experienced large deformation. F_p thereof raises constantly up to about 0.32, which means significant particle rotation takes place inside the packing. F_c, on the other hand, reaches a plateau of 0.6 at $\varepsilon_q = 4\%$ and stays steady until $\varepsilon_q = 14\%$, after which a rise of F_c is observed due to the loss of contact in the packing. The fabric responses of the RVE at point B outside SB (when the deviatoric strain level is small ($\varepsilon_q < 9\%$)) and inside SB are similar to those at point A. For the RVEs at point A outside SB under the light and the heavy foundations, the increase of F_c is almost linear following an apparent reversal due to unloading. Since the volume change in these two cases is small ($|\varepsilon_V| < 0.12\%$ shown in Fig. 5(b)), F_p remains almost stagnant as there is not sufficient extra space for particles to rotate.

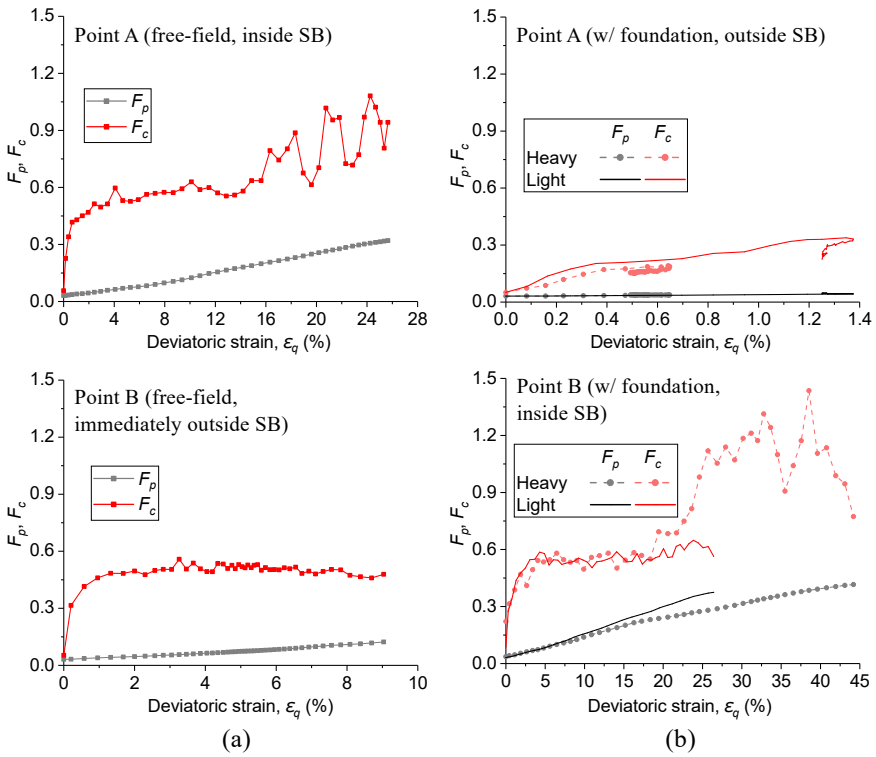

Fig. 6. Fabric evolution of the two selected RVEs embedded at points A and B: (a) free-field; (b) heavy and light foundations.

5 CONCLUSIONS

A multiscale approach coupling FEM and DEM is utilized to simulate the normal fault rupture propagation and FR-SFI. In the free-field case, the fault rupturing paths through the sand layer and the induced ground displacements are well captured generally agreeing with those observed in the centrifuge tests [6] and predicted by other numerical studies [8, 11]. The study of FR-SFI problems reveals that the fault rupturing direction could be diverted from that in the free-field due to the presence of shallow foundations. In addition, multiscale analyses are conducted by examining the responses and microstructural evolutions of selected local RVE packings. It is found that the RVEs located in- or outside SBs can have very distinct behaviors, and may change from the initial at-rest state to the active state in the normal fault case. The micromechanics study also reports the possible detriment of heavy foundations for the superstructure despite the rupture surface diversion. Further study may consider using more realistic soil-foundation contact models applying interface and tension cut-off to replace the sticking assumption in simulating FR-SFI.

ACKNOWLEDGEMENTS

The study was financially supported by the National Natural Science Foundation of China (Nos. 52078456, 51809229, 52020105003) and the Fundamental Research Funds for the Central Universities, China (No. 2021FZZX001-14).

REFERENCES

[1] Bray, J.D., Seed, R.B. and Seed, H.B. Analysis of earthquake fault rupture propagation through cohesive soil. *J. Geotech. Eng.* (1994) **120** (3): 562–580.

[2] Bray, J.D. Developing mitigation measures for the hazards associated with earthquake surface fault rupture. *In Proc., Workshop on Seismic Fault-Induced Failures—Possible Remedies for Damage to Urban Facilities,* edited by K. Konagai, 55–79. Tokyo: Univ. of Tokyo, (2001).

[3] Stirling, M.W., et al. The Mw 7.8 2016 Kaikōura earthquake: Surface fault rupture and seismic hazard context. *Bull. N. Z. Soc. Earthquake Eng.* (2017) **50** (2): 73–84.

[4] Cai, Q.P. and Ng, C.W.W. Centrifuge modeling of pile-sand interaction induced by normal faulting. *J. Geotech. Geoenviron. Eng.* (2016) **142** (10): 04016046.

[5] Yao, C., and J. Takemura. Centrifuge modeling of single piles in sand subjected to dip-slip faulting. *J. Geotech. Geoenviron. Eng.* (2020) **146** (3): 04020001.

[6] Bransby, M.F., Davies, M.C. and Nahas, A.EI. Centrifuge modelling of normal fault–foundation interaction. *Bull. Earthquake. Eng.* (2008) **6**: 585-605.

[7] Anastasopoulos, I., Gazetas, G., Bransby, M.F., Davies, M.C. and Nahas, A. El. Normal fault rupture interaction with strip foundations. *J. Geotech. Geoenviron. Eng.* (2009) **135** (3): 359–370.

[8] Oettle, N. K. and Bray, J. D. Numerical procedures for simulating earthquake fault rupture propagation. *Int. J. Geomech.* (2016) **17** (1): 04016025.

[9] del Castillo, E.M., Fávero Neto, A.H. and Borja, R.I. Fault propagation and surface rupture in geologic materials with a meshfree continuum method. *Acta Geotech.* (2021) **16** (8): 2463–2486.

[10] Hazeghian, M. and Soroush, A. Numerical modeling of dip-slip faulting through granular

soils using DEM. *Soil Dyn. Earthquake Eng.* (2017) **97**: 155–171.
[11] Garcia, F.E., and Bray, J.D. Discrete element analysis of earthquake fault rupture-soil foundation interaction. *J. Geotech. Geoenviron. Eng.* (2019a) **145** (9): 04019046.
[12] Garcia, F.E. and Bray, J.D. Discrete-element analysis of influence of granular soil density on earthquake surface fault rupture interaction with rigid foundations. *J. Geotech. Geoenviron. Eng.* (2019b) **145** (11), 04019093.
[13] Guo, N. and Zhao, J.D. A coupled FEM/DEM approach for hierarchical multiscale modelling of granular media. *Int. J. Numer. Meth. Eng.* (2014) **99**(11):789-818.
[14] Zhao, S.W. and Zhao, J.D. SudoDEM: Unleashing the predictive power of the discrete element method on simulation for non-spherical granular particles. *Comput. Phys. Comm.* (2021) **259**: 107670.
[15] Kruyt, N.P., and Rothenburg, L. Statistical theories for the elastic moduli of two-dimensional assemblies of granular materials. *Int. J. Eng. Sci.* (1998) **36** (10): 1127–1142.
[16] Zhao, J.D. and Guo, N. The interplay between anisotropy and strain localisation in granular soils: a multiscale insight. *Géotechnique* (2015) **65** (8): 642–656.
[17] Guo, N., Chen, L.F. and Yang, Z.X. Multiscale modelling and analysis of footing resting on an anisotropic sand. *Géotechnique* (2022) **72** (4): 364–376.
[18] Bolton, M.D. The strength and dilatancy of sands. *Géotechnique* (1986) **36** (1): 65–78.
[19] Desrues, J., Argilaga, A., Caillerie, D., Combe, G., Nguyen, T.K., Richefeu, V. and Dal Pont, S. From discrete to continuum modelling of boundary value problems in geomechanics: an integrated FEM-DEM approach. I*nt. J. Numer. Anal. Methods Geomech.* (2019) **43** (5): 919–955.
[20] Yao, C., Takemura, J., Ma, G., Dai, C. and An, Z. Effect of boundary friction on reverse fault rupture propagation in centrifuge tests. *Soil Dyn. Earthquake Eng.* (2021) **147**: 106811.